JPn Neuroscience

The Journal of Physiology

J Physiol 590.19 (2012) pp 4801–4818

Control of neuronal excitability by NMDA-type glutamate receptors in early developing binaural auditory neurons

Jason Tait Sanchez[1,2], Armin H. Seidl[1,2], Edwin W. Rubel[1,2,3] and Andres Barria[1,3]

[1] *Virginia Merrill Bloedel Hearing Research Center,* [2] *Otolaryngology – Head & Neck Surgery and* [3] *Department of Physiology and Biophysics, University of Washington, Seattle, WA, USA*

Key points

- Mature nucleus laminaris (NL) neurons in the avian auditory brainstem respond with one or two action potentials to repetitive synaptic stimulation due to strong expression of low-voltage-activated K^+ channels (K_{LVA}) and other intrinsic factors.
- We observe early in development, before the onset of hearing, NL neurons respond in similar fashion despite low expression of K_{LVA} channels. At this age, synaptic NMDA-type glutamate receptors (NMDA-Rs) contain primarily the GluN2B subunit, which allow the summation of synaptic responses and keep voltage-dependent Na^+ channels inactivated.
- Weaker Mg^{2+} blockade of NMDA-Rs and an immature reuptake system cause a tonic NMDA-R-mediated current that sets the membrane potential at more depolarized values. Small K_{LVA} conductances localized in dendrites prevent ramping depolarization and excessive excitability.
- Our data show that before intrinsic properties are fully developed, NMDA-Rs limit the output of NL neurons.

Abstract Precise control of neuronal excitability in the auditory brainstem is fundamental for processing timing cues used for sound localization and signal discrimination in complex acoustic environments. In mature nucleus laminaris (NL), the first nucleus responsible for binaural processing in chickens, neuronal excitability is governed primarily by voltage-activated potassium conductances (K_{VA}). High levels of K_{VA} expression in NL neurons result in one or two initial action potentials (APs) in response to high-frequency synaptic activity or sustained depolarization. Here we show that during a period of synaptogenesis and circuit refinement, before hearing onset, K_{VA} conductances are relatively small, in particular low-voltage-activated K^+ conductances (K_{LVA}). In spite of this, neuronal output is filtered and repetitive synaptic activity generates only one or two initial APs during a train of stimuli. During this early developmental time period, synaptic NMDA-type glutamate receptors (NMDA-Rs) contain primarily the GluN2B subunit. We show that the slow decay kinetics of GluN2B-containing NMDA-Rs allows synaptic responses to summate, filtering the output of NL neurons before intrinsic properties are fully developed. Weaker Mg^{2+} blockade of NMDA-Rs and ambient glutamate early in development generate a tonic NMDA-R-mediated current that sets the membrane potential at more depolarized values. Small K_{LVA} conductances, localized in dendrites, prevent excessive depolarization caused by tonic activation of NMDA-Rs. Thus, before intrinsic properties are fully developed, NMDA-Rs control the output of NL neurons during evoked synaptic transmission.

(Received 20 January 2012; accepted after revision 19 July 2012; first published online 23 July 2012)
Corresponding author A. Barria: Physiology and Biophysics, School of Medicine, University of Washington, Box 357290, Seattle, WA 98195, USA. Email: barria@u.washington.edu

Abbreviations AP, action potential; ATDP, after-train depolarizing plateau; K_{VA}, voltage-activated K^+ conductance; K_{LVA}, low voltage-activated K^+ conductance; MSO, medial superior olive; NL, nucleus laminaris; NM, nucleus magnocellularis.

DOI: 10.1113/jphysiol.2012.228734

Introduction

The auditory system is capable of extracting information from incoming signals to accurately locate the source of a sound. Prominent is the ability to process the horizontal location of low-frequency sounds, which depends on the accuracy of encoding time differences in the order of ten to a few hundred microseconds in the arrival of auditory cues at the two ears. In the auditory brainstem of both birds and mammals, neurons possess highly specialized anatomical and physiological properties that allow them to encode these submillisecond time differences (for review see Burger & Rubel, 2008).

The control of neuronal excitability is a physiological property fundamental for encoding timing differences in both birds and mammals. In mature nucleus laminaris (NL), the avian analog to the mammalian medial superior olive (MSO), excitability is governed primarily by the site of axonal action potential (AP) initiation (Kuba *et al.* 2006, 2010) and by voltage-activated potassium K^+ channels (K_{VA}), often resulting in the generation of one or two initial APs in response to sustained depolarization or repetitive stimulation (Reyes *et al.* 1996; Kuba *et al.* 2002, 2003). The generation of one or two APs is necessary for optimizing well-timed converging inputs, allowing NL neurons to act as coincidence detectors of binaural auditory information (Carr & Konishi, 1990; Joseph & Hyson, 1993; Pena *et al.* 2001). This specialization is also found in time-coding auditory neurons of mammals (Brew & Forsythe, 1995; Oertel, 1991, 1997; Rothman & Manis, 2003; Barnes-Davies *et al.* 2004; Scott *et al.* 2005; Mathews *et al.* 2010).

Before hearing onset and during a period of synaptogenesis in NL, factors controlling neuronal excitability are less clear. During this early developmental period, the expression of K_{VA} is low, increasing dramatically as the system matures and hearing emerges (Kuba *et al.* 2002; Gao & Lu, 2008). Parallel to changes in K_{VA} expression, the subunit composition of synaptic NMDA-type glutamate receptors (NMDA-Rs) change from GluN2B-containing receptors before hearing onset to GluN2A-containing receptors once the system has approached functional maturity (Sanchez *et al.* 2010). This switch in NMDA-R subunit composition changes the fractional Ca^{2+} current influx (Burnashev *et al.* 1995; Sobczyk *et al.* 2005) and the temporal activation profiles (Erreger *et al.* 2005), accelerating the kinetics of NMDA-R-mediated excitatory postsynaptic currents (EPSCs) (Flint *et al.* 1997; Stocca & Vicini, 1998).

During the past decade, it has become increasing clear that NMDA-Rs contribute to information transfer at synapses in mature auditory nuclei in a variety of ways, including regulating firing probability, response latency, spike jitter, temporal patterning and long-term potentiation (cochlear nucleus, Pliss *et al.* 2009; superior olive, Steinert *et al.* 2010; lateral lemniscus, Sivaramakrishnan & Oliver, 2006; Porres *et al.* 2011; inferior colliculus, Wu *et al.* 2004; Sanchez *et al.* 2007; medial geniculate, Bartlett & Smith, 2002; auditory cortex, Hogsden & Dringenberg, 2009). However, despite several reports establishing their abundance in early auditory development (Taschenberger & von Gersdorff, 2000; Futai *et al.* 2001; Tang & Carr, 2004, 2007; Lu *et al.* 2007; Gao & Lu, 2008; Sanchez *et al.* 2010) the functional role of NMDA-Rs before hearing onset is less established.

Here we sought to determine the functional role of NMDA-Rs during early auditory development in the chicken NL. We show that long-lasting NMDA-R currents filter the neuronal output of NL neurons during a pre-hearing period when synapses are recently formed. This filtering results in the generation of only one or two initial APs in response to a train of repetitive synaptic stimulation. During this period, K_{VA} channels are not yet fully expressed and the control of neuronal excitability is due to NMDA-Rs containing the GluN2B subunit. Minimal expression of low-voltage-activated K^+ conductances (K_{LVA}), one of which is located primarily in dendrites, contributes to prevent run-away depolarization caused by extracellular glutamate and a weaker Mg^{2+} blockade of NMDA-Rs during early NL development.

It is established that the filtering of neuronal output in mature NL neurons is necessary for binaural hearing (for review see Burger & Rubel, 2008). In early developing NL, however, synaptic responses mediated by GluN2B-containing NMDA-Rs may be required for sculpting NL specializations important for encoding binaural cues found in mature auditory neurons, while the filtering of neuronal output may assist in the selection of appropriate synapses and circuit refinement.

Method

Slice preparation

Acute brainstem slices were prepared from White Leghorn chicken (*Gallus domesticus*) at embryonic (E) days 19 and E11 as described previously (Sanchez *et al.* 2010). All procedures were approved by the University of Washington Institutional Animal Care and Use Committee and conformed to NIH guidelines. Efforts were made to minimize pain or discomfort of the animals and to minimize the number of the animals used. Briefly, the brainstem was dissected and isolated in ice-cold (~0°C) oxygenated low-Ca^{2+} high-Mg^{2+} modified artificial cerebral spinal fluid (ACSF) containing the following (in mM): 130 NaCl, 3 KCl, 1.25 NaH_2PO_4, 26 $NaHCO_3$, 4 $MgCl_2$, 1 $CaCl_2$ and 10 glucose. ACSF was continuously bubbled with a mixture of 95% O_2–5% CO_2 (pH 7.4, osmolarity 295–310 mosmol l^{-1}). The brainstem was blocked coronally, affixed to the stage of a

vibratome slicing chamber (Technical Products International, St Louis, MO, USA) and submerged in ice-cold ACSF. Bilaterally symmetrical coronal slices were made (200–300 μm thick) and approximately three to six slices (depending on age) containing NM and NL were taken from caudal to rostral, roughly representing the low- to high-frequency regions of NL, respectively. All neurons reported here were obtained from the rostral one-third of the entire nucleus, roughly representing the high-frequency region of NL. This region was selected in order to minimize effects of membrane capacitance and dendritic filtering on neuronal response properties.

Slices were collected in a holding chamber and allowed to equilibrate for 1 h at 36°C in normal ACSF containing the following (in mM): 130 NaCl, 3 KCl, 1.25 NaH_2PO_4, 26 $NaHCO_3$, 1 $MgCl_2$, 3 $CaCl_2$ and 10 glucose. Normal ACSF was continuously bubbled with a mixture of 95% O_2–5% CO_2 (pH 7.4, osmolarity 295–310 mosmol l^{-1}). Slices were allowed to cool to room temperature for 30 min before being transferred from the holding chamber to a 0.5 ml recording chamber mounted on an Olympus BX51W1 (Center Valley, PA, USA) microscope for electrophysiological experiments. The microscope was equipped with a CCD camera, 60× water-immersion objective and infrared differential interference contrast optics. The recording chamber was superfused continuously at near-physiological temperatures (monitored at ∼33–35°C) in oxygenated normal ACSF at a rate of 1.5–2 ml min^{-1}.

Whole-cell electrophysiology

Voltage-clamp and current-clamp experiments were performed using an Axon Multiclamp 700B amplifier (Molecular Devices). Patch pipettes were pulled to a tip diameter of 1–2 μm and had resistances ranging from 3 to 6 MΩ. For voltage-clamp experiments, the internal solution was cesium-based containing the following (in mM): 108 $CsMeSO_3$, 5 CsCl, 1 $MgCl_2$, 15 phosphocreatine-$Tris_2$, 8 BAPTA-Cs_4, 10 Hepes, 3 QX-314.Cl, 4 MgATP and 0.4 $Tris_2$GTP, pH adjusted to 7.3 with TrisOH. The liquid junction potential was 5 mV and data were adjusted accordingly. The Cs-based internal solution was used to block K^+ conductances and QX-314. Cl was used to block Na^+ conductances in an attempt to reduce space-clamp issues associated with dendritic filtering. Series resistance was compensated for by ∼80% in all voltage-clamp recordings. For current-clamp experiments, the internal solution was potassium-based containing the following (in mM): 105 potassium gluconate, 35 KCl, 1$MgCl_2$, 10 Hepes-K^+, 5 EGTA, 4 ATP-Mg^{2+} and 0.3 GTP-Na^+, pH adjusted to 7.3 with KOH. The liquid junction potential was 10 mV and data were adjusted accordingly.

A small hyperpolarizing (−1 mV, 100 ms) voltage command was presented at the beginning of each recorded trace to document and monitor whole-cell parameters (resting membrane potential (RMP), cell membrane capacitance, series resistance and input resistance). RMPs were measured immediately after break-in to avoid cesium-induced depolarization during voltage-clamp experiments. Neurons were included in the data analysis only if they had RMPs between −50 mV and −70 mV and had series resistances <15 MΩ. Raw data were low-pass filtered at 2 kHz and digitized at 20 kHz using a Digidata 1440A (Molecular Devices).

Pipettes were visually guided to NL and neurons were identified and distinguished from surrounding tissue based on cell morphology, known laminar structure and location of the nucleus within the slice. All experiments were conducted in the presence of a $GABA_A$-R antagonist picrotoxin (PTX, 100 μM). After a gigaohm seal was attained, membrane patches were ruptured and NL neurons were held in whole-cell configuration for voltage-clamp recordings at membrane potentials ranging between −90 mV and +40 mV (dependent on experimental protocol). For current-clamp experiments, NL neurons were held in whole-cell configuration at $I = 0$ for recording intrinsic and synaptic membrane potentials. Isolated AMPA-R-mediated EPSCs were recorded in the presence of the NMDA-R antagonist DL-2-amino-5-phosphonopentanoic acid (DL-APV, 100 μM). Isolated NMDA-R-mediated EPSCs were recorded in the presence of the AMPA-R antagonist 1,2,3,4-tetrahydro-6-nitro-2,3-dioxo-benzo[f]quinoxaline-7-sulfonamide disodium salt hydrate (NBQX, 20 μM). Isolated K^+ currents were recorded in the presence of the Na^+ channel blocker tetrodotoxin (TTX, 1 μM), NBQX and DL-APV. Dendrotoxin (DTX-I, 0.1 μM) and Fluoxetine (100 μM) were used to selectively block low- and high-voltage-activated K^+ currents, respectively. K^+ leak currents were not subtracted from the raw data but were estimated offline using the responses to the hyperpolarizing steps from −80 to −90 mV as a baseline.

Synaptic inputs from only one side of the brainstem (ipsilateral synaptic stimulation) were stimulated using a concentric bipolar electrode (tip core diameter, 200 μm, World Precision Instruments, Sarasota, FL, USA). Square electric pulses, 100 μs in duration, were delivered by an Iso-flux stimulator (AMPI; Jerusalem, Israel) and interval generator (S88; Grass, West Warwick, RI, USA). Stimulating electrodes were placed in the ipsilateral dorsal neuropil region of NL, approximately 30–50 μm from the NL neurons being studied. Stimulus intensity was gradually adjusted until responses were reliably elicited such that postsynaptic events were of maximal amplitude and no failures occurred. To evoke EPSPs, stimulus intensity was adjusted to half the strength needed to elicit APs and then TTX was added to the bath to ensure only

EPSPs were measured. The after-train depolarizing plateau (ATDP) was measured 50 ms after the final pulse in the stimulus train and averaged across a 10 ms time window.

Data analysis

Recording protocols were written and run using Clampex acquisition and Clampfit analysis software (version 10.1; Molecular Devices). Statistical analyses and graphing protocols were performed using Prism (GraphPad versions 5.0a, La Jolla, CA, USA). The standard for significant differences was defined as $P < 0.05$. All graphic representations of data illustrate mean ± 1 standard error of the mean (SEM).

Reagents

All bath-applied drugs were allowed to perfuse through the recording chamber for ∼2 min before subsequent recordings. DL-threo-β-benzyloxyaspartate (TBOA, 100 μM, glial and neuronal glutamate uptake blocker), DL-APV, NBQX and all other salts and chemicals were obtained from Sigma-Aldrich (St Louis, MO, USA). DTX-I, PTX and Fluoxetine were obtained from Tocris (Ellisville, MI, USA). TTX and QX-314 were obtained from Alomone Labs (Jerusalem, Israel).

Anti-Kv1.2 immunoreactivity

E19 ($n = 3$) and E11 ($n = 2$) chicken brains were fixed in a 4% paraformaldehyde (PFA) and phosphate buffer (0.1 M, pH 7.4) overnight at 4°C. Brains were rinsed in phosphate-buffered saline (PBS) and embedded in 5% agar. Sections 35 μm thick containing NL and NM were prepared with a vibratome (Leica VT 1000S, Leica Microsystems). Sections were immunolabelled with 1:1000 anti-Kv1.2 potassium channel subunit antibody (NeuroMab clone K14/16) in PBS with a standard block solution for at least 6 h at room temperature (RT) or overnight at 4°C. After rinsing, sections were exposed to the secondary antibody (1:500, Alexa Fluor 594 goat anti-mouse, Invitrogen) overnight at 4°C in standard block solution. After rinsing, sections were coverslipped with Glycergel (Dako) and imaged using a confocal microscope (Fluoview 1000, Olympus). Intensity profile pictures generated from a 3-D image stack were made with Huygens software (Scientific Volume Imaging).

Single-cell dye electroporation with Kv1.2 immunoreactivity

Acute brainstem slices of E19 ($n = 2$) and E11 ($n = 2$) chicken were prepared as described above. Single NL neurons were electroporated with Alexa 488 dextran dye as described previously (Sorensen & Rubel, 2006; Seidl *et al.* 2010). Briefly, under a microscope, a pipette tip (diameter 1–2 μm) filled with 20 mM Alexa dextran dye was placed near the soma of an individual NL neuron in an acute slice maintained in normal ACSF. A brief train of square pulses (100 μs pulse, 10–50 mV) was applied to fill individual neurons with the Alexa dextran dye. Immediately after electroporation, slices were fixed in 4% PFA at RT for 15–30 min. Slices then underwent the Kv1.2 staining protocol described above. Slices were embedded between two coverslips in Glycergel to ensure imaging from both sides. Filled neurons labelled with the Kv1.2 antibody were imaged by confocal microscopy and the 3-D images were deconvolved, Gaussian filtered and surface rendered using Huygens software.

Results

We recorded from a total of 97 NL neurons obtained from acute brainstem slices prepared at embryonic (E) day 19 (E19, $n = 40$ neurons) and E11 ($n = 67$ neurons) chicken embryos. These ages correspond to developmental time periods when functional properties are considered mature-like (E19) and when synapses are becoming established prior to the onset of hearing (E11) (Rubel & Parks, 1988). Below we describe the role of NMDA-Rs and voltage-activated K^+ channels in the control of neuronal excitability during a period of synaptogenesis and circuit refinement.

Single action potential (AP) generation in response to sustained synaptic activation in developing NL neurons

When afferent inputs to E19 NL neurons were stimulated with 10 pulses delivered at a rate of 100 Hz, a frequency of physiological relevance (Born *et al.* 1991), the postsynaptic neurons responded with one or two APs that were always triggered by the first or second stimulus of the train (Fig. 1). Repetitive stimulation to one set of inputs always elicited a single AP in response to the first stimulus (Fig. 1*A*). The occurrence of a second AP to the second stimulus pulse was occasionally observed with a probability of ∼0.3 (Fig. 1*B*). This result is consistent with previous reports for mature NL neurons (Kuba *et al.* 2002) and other auditory brainstem nuclei that encode timing cues used for binaural hearing (Oertel, 1991, 1997; Brew & Forsythe, 1995; Taschenberger & von Gersdorff, 2000; Futai *et al.* 2001). No AP occurred in the last eight pulses of the stimulus train (Fig. 1*B*). Since APs that occurred to the second stimulus pulse exhibited variable peak amplitudes (Kuba *et al.* 2002), three criteria were used to distinguish APs from EPSPs: (1) the presence of an abrupt inflection

or shoulder in the rising phase of the response (threshold); (2) a peak amplitude >30 mV from the threshold of spike initiation; and (3) a half-width (duration of the AP at half-maximal amplitude) <4 ms for E11 neurons and <1 ms for E19 neurons (Gao & Lu, 2008).

Surprisingly, immature NL neurons (E11) also responded with one or two APs when afferent inputs were rapidly stimulated (10 pulses at a rate of 100 Hz; 10 trials repeated once every 10 s; Fig. 1*C*). Similar to E19 neurons, all APs from E11 NL neurons were generated either after the first or within the first two stimulus pulses (only one E11 NL neuron generated three APs, all occurring within the first three stimulus pulses). Similar to E19 neurons, no AP occurred in the last seven to eight pulses of the stimulus train (Fig. 1*D*). In contrast to E19 neurons, however, all E11 neurons maintained a depolarized state during the later segment of the train. This resulted in a strong depolarizing plateau that lasted hundreds of milliseconds after the stimulus train. We termed this sustained response as the *after-train depolarizing plateau* (ATDP).

It is well established that in mature NL neurons the generation of one or two APs after sustained synaptic activation to one set of inputs (Kuba *et al.* 2002) or constant depolarization (Reyes *et al.* 1996) is due to a combination of pre- and postsynaptic mechanisms, as well as intrinsic properties of NL neurons. In particular, large conductances mediated by K_{LVA} channels increase the threshold for AP generation and reduce the time constant of the membrane, consequently reducing the time window during which inputs can summate and effectively controlling neuronal excitability. It is unclear what contributes to the control of neuronal excitability during early NL development.

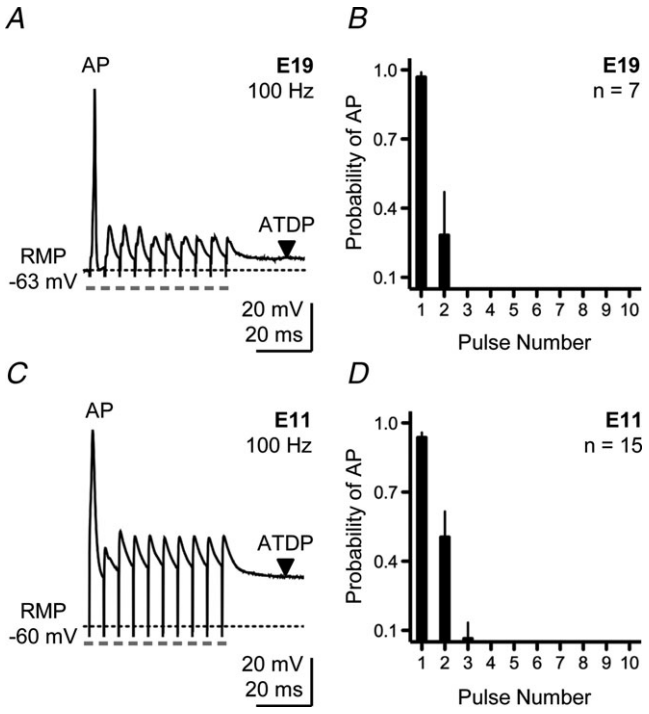

Figure 1. Single action potential generation in response to sustained synaptic activation in developing NL neurons
A, representative current-clamp trace for an E19 NL neuron elicited by a train of 10 pulses delivered at a rate of 100 Hz. Pulse train repeated every 10 s. *B*, population data for E19 NL neurons showing the probability of action potential occurrence as a function of pulse number during a 100 Hz train. *C*, representative current-clamp trace for an E11 NL neuron elicited by a train of 10 pulses delivered at a rate of 100 Hz. Pulse train repeated every 10 s. *D*, population data for E11 NL neurons showing the probability of action potential occurrence as a function of pulse number during a 100 Hz train. In this and subsequent figures: RMP, resting membrane potential; AP, action potential; ATDP, after-train depolarizing potential, downward arrowhead. Dashed lines in traces represent baseline RMP. Grey rectangles under traces represent time point of stimulus pulse. Stimulus artifacts not removed. Data represent mean ± SEM.

Minimal contribution of low-voltage-activated potassium currents early in development

Voltage-activated K^+ currents – both low- and high-voltage dependent – are developmentally up-regulated in NL (Gao & Lu, 2008). Similar to previous reports, we observed a 3-fold increase in total K^+ current from E11 to E19 (Fig. 2*A*–*C*). Neurons were voltage-clamped at −60 mV and stepped from −90 mV to +20 mV in 5 mV increments (200 ms duration) and the average steady-state current between 180 and 185 ms of the voltage command was measured and used to derive the *I*–*V* relationship shown in Fig. 2*C*. In E19 neurons, ∼79% of the total K^+ current was sensitive to bath application of DTx-I (0.1 μM, data not shown), a specific blocker against the low-voltage-activated Kv1.1- and Kv1.2-containing channels (Johnston *et al.* 2010; Mathews *et al.* 2010). This finding is in close agreement with other studies performed in mammals (Scott *et al.* 2005; Johnston *et al.* 2010; Mathews *et al.* 2010) and confirms a dominant role of K_{LVA} conductances in mature NL neurons.

In contrast, E11 NL neurons not only exhibited reduced potassium currents compared with E19, but we also found a minimal contribution of K_{LVA} current at this early age relative to K_{HVA}. Figure 2*D* shows representative voltage-clamp traces of isolated K^+ currents for an E11 NL neuron before (black traces) and after (grey traces) bath application of 0.1 μM DTx-I. There was negligible reduction in the total amount of K^+ current elicited by the hyperpolarizing and depolarizing voltage commands with bath application of DTx-I (Fig. 2*D* and *E*). However, when measured between −55 mV and −30 mV (Fig. 2*E*, grey shaded region), approximately 33% of the total K^+ current was sensitive to DTx-I application (Fig. 2*E*, inset), suggesting some minimal contribution of K_{LVA} to the total K^+ current measured at E11.

Bath application of Fluoxetine (FLx, 100 μM), a highly specific open channel blocker for Kv3.1-containing, high-voltage-activated K^+ channels (K_{HVA}) (Sung *et al.* 2008), significantly reduced the total amount of K^+ current in E11 NL neurons. Figure 2*F* shows representative voltage-clamp traces of isolated K^+ currents recorded before (black traces) and after (grey traces) bath application of FLx for a different E11 NL neuron. FLx application caused a minimal reduction in the total amount of K^+ current measured at −40 mV, but a large reduction at +20 mV (Fig. 2*G*), suggesting a strong contribution of the K_{HVA} channel at this age. A similar

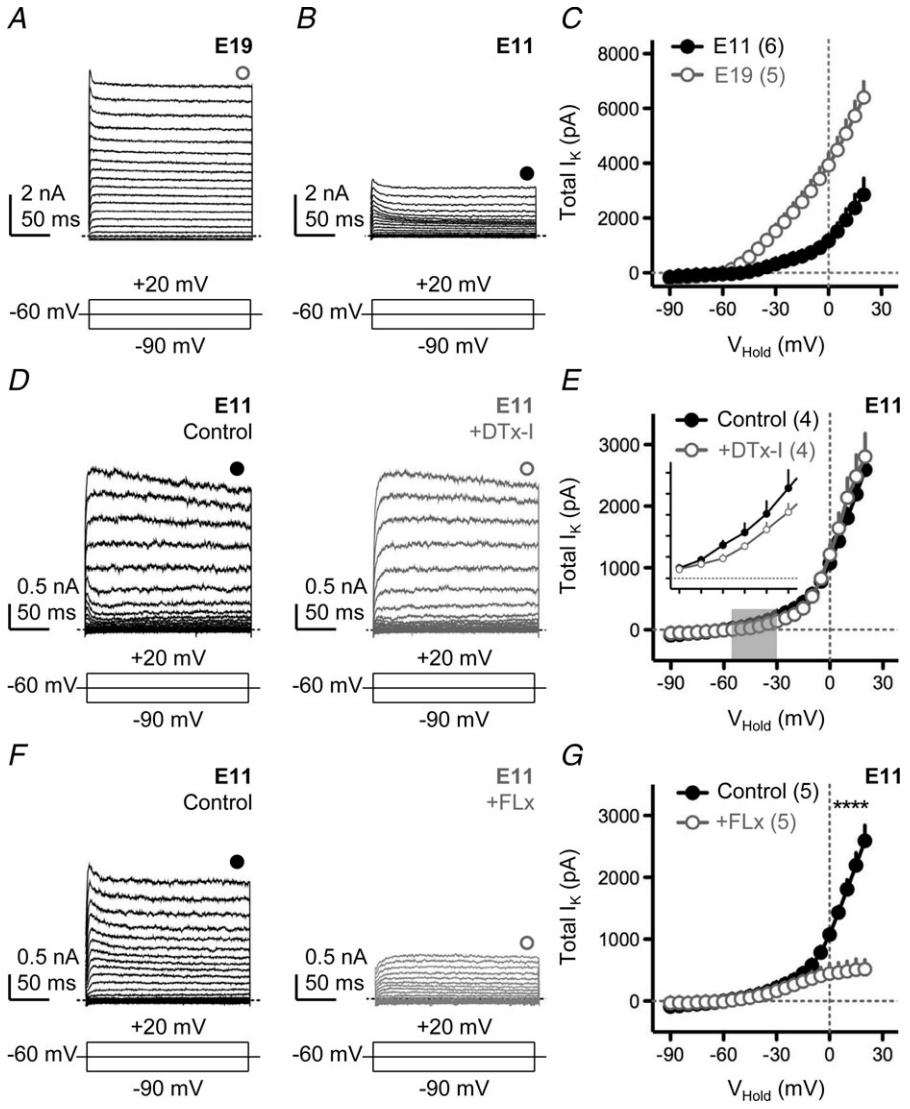

Figure 2. Minimal contribution of low-voltage-activated potassium currents early in development
A and *B*, representative voltage-clamp traces of isolated K^+ currents for E19 (*A*) and E11 (*B*) NL neurons. *C*, population current–voltage (*I–V*) curves for E19 and E11 NL neurons. *D*, representative voltage-clamp traces of isolated K^+ currents for an E11 NL neuron before (left, black traces) and after (right, grey traces) bath application of a specific K_{LVA} blocker (DTx-I, 0.1 μM). *E*, population *I–V* curves for E11 neurons before and after DTx-I application. Grey shaded region indicates voltage range (−55 mV to −30 mV) used to determine the average amount of K^+ current that was sensitive to bath application of DTx-I (inset). Inset *Y*-axis tick marks are 0 to 250 pA in steps of 50 pA: *X*-axis are −55 to −30 mV in steps of 5 mV. *F*, representative traces for another E11 NL neuron before (left, black traces) and after (right, grey traces) application of a specific K_{HVA} blocker (FLx, 100 μM). *G*, population *I–V* curves for E11 before and after FLx. In *A*, *B*, *D* and *F*, neurons were held at −60 mV and stepped from −90 mV to +20 mV (steps of 5 mV, duration 200 ms). Schematic lines under traces represent the holding, minimal and maximal voltages (minimized for clarity) injected into the soma. Filled and open circles above traces represent time point taken (averaged across 5 ms) to construct steady-state *I–V* curves shown in *C*, *E* and *G*. All experiments were performed in the presence of DNQX, DL-APV, PTX and TTX. In this and subsequent figures: $^*P < 0.05$, $^{**}P < 0.01$, $^{***}P < 0.001$, paired *t* test. Numbers in parentheses, *n*.

result was obtained with a low concentration of tetraethyl ammonium (TEA, 1 mM; data not shown), known to be relatively effective at blocking Kv3-containing channels (Johnston *et al.* 2010). These functional results are in close agreement with the expression pattern of K_{HVA} channels during early NL development (Parameshwaran-Iyer *et al.* 2003). These results also indicate that there is less total K^+ channel current at E11 compared with E19. More significantly, there is a minimal contribution of the K_{LVA} channel relative to K_{HVA} early in development of NL neurons.

Developmental differences in excitatory postsynaptic potentials (EPSPs) following afferent stimulation

Despite a minimal contribution of K_{LVA} conductances at E11, NL neurons still respond with one or two APs to sustain synaptic activity. Important differences are observed in synaptically evoked sub-threshold post-synaptic potentials (EPSPs) between developing E11 neurons and mature-like E19 neurons in NL.

Low-frequency stimulation (0.1 Hz) of afferent fibres into mature E19 NL neurons triggered extremely rapid EPSPs (Fig. 3*A*). The average width of this EPSP, measured at half-maximal amplitude, was 1.86 ± 0.23 ms ($n = 5$ neurons), in close agreement with other stage-matched time-coding auditory neurons (Scott *et al.* 2005; Gao & Lu, 2008). In addition, the width of the EPSP at this age was shaped primarily by the presence of strong K_{LVA} conductances (data not shown). In contrast, synaptically evoked EPSPs recorded from E11 NL neurons were significantly slower ($P < 0.001$), with an average width of 43.86 ± 7.82 ms ($n = 5$ neurons; Fig. 3*B*), suggesting the relatively minimal contribution of K_{LVA} conductances at this age. These results were consistent across the population of neurons tested at both ages (Fig. 3*C*).

In mature NL neurons, repetitive subthreshold afferent stimulation (10 pulses at a rate of 100 Hz; 10 trials repeated once every 10 s) resulted in EPSPs that depressed as the train of stimuli progressed (Fig. 3*D*). In contrast, for the E11 NL neuron in Fig. 3*E*, the EPSPs were not depressed but summated following rapid afferent stimulation, resulting in a strong ATDP. This ATDP is clearly visible when E11 NL neurons were stimulated with an AP-inducing train as shown in Fig. 1*C*. The average ATDP was measured 50 ms after the final pulse in the train and averaged across a 10 ms time window. In E11 neurons, ATDP was 12.80 ± 3.81 mV above the starting resting membrane potential (RMP; $n = 5$ neurons) and was more than double than the ATDP measured at E19 (4.88 ± 2.09 mV; $n = 5$ neurons, $P < 0.01$). These results were consistent across the population of neurons tested at both ages (Fig. 3*F*).

Developmental differences in excitatory postsynaptic currents (EPSCs) following rapid afferent stimulation

Previous studies from our group and others have shown dramatic changes in the kinetics and sub-unit composition of NMDA- and AMPA-Rs in nucleus magnocellularis (NM) and NL across the ages studied. NL neurons change from containing the GluN2B sub-unit at E11 to GluN2A-containing receptors at E19. This change in subunit composition accelerates the kinetics of NMDA-R-mediated EPSCs (Sanchez *et al.* 2010). Similarly, developing AMPA-R-mediated currents in NL change from GluA2-containing receptors at E11 to GluA2-lacking receptors at E19, resulting in significantly faster kinetics of AMPA-R-mediated EPSCs (Sanchez *et al.* 2010). Similar findings have been described in NM (Lu *et al.* 2007) and other auditory brainstem nuclei (Taschenberger & von Gersdorff, 2000; Futai *et al.* 2001).

To better identify the source responsible for the differences in the generation of EPSPs following afferent synaptic stimulation, we analysed the underlying synaptic currents following a train of 10 stimuli delivered at a rate of 100 Hz. To address a potential role of AMPA-Rs in contributing to the developmental differences in synaptically triggered postsynaptic potentials, we isolated AMPA-R current responses recorded at negative holding potentials (−60 mV) and in the presence of the NMDA-R antagonist DL-APV (100 μM). As shown in Fig. 4*A* for an E19 NL neuron (superimposed grey trace), considerable depression is seen during the rapid stimulus train. This type of synaptic depression is consistent in mammals and birds (for reviews see Trussell, 1998, 1999) and is probably due to presynaptic mechanisms (Stevens & Wang, 1995) as well as AMPA-R desensitization (Hestrin, 1992). Surprisingly, a similar amount of synaptic depression was recorded for the E11 NL neuron shown in Fig. 4*A* (black trace). Although synaptic depression of isolated AMPA-R-mediated EPSCs was largest for E19 neurons, it was not significantly different from E11 neurons (Fig. 4*B*). This indicates that the slower GluA2-containing AMPA-Rs present at E11 (Sanchez *et al.* 2010) do not contribute to the summation of EPSPs elicited by a train of rapid afferent stimulation.

When isolated NMDA-R responses were recorded at positive holding potentials (+40 mV) and in the presence of the AMPA-R antagonist NBQX (20 μM), we observed minimal facilitation following the second and third stimulus pulse for the E19 NL neuron shown in Fig. 4*C* (superimposed grey trace). Moreover, a clear depression for the remaining stimulus pulses in the train was observed across the population of E19 NL neurons tested (Fig. 4*C* and *D*). In marked contrast, a 2.5-fold increase in the NMDA-R-mediated EPSC at E11 was observed from the first EPSC to the last EPSC triggered by the rapid train of afferent stimulation for the neuron shown in Fig. 4*C*

(superimposed black trace). This significant summation of the isolated NMDA-R-mediated current was evident across the population of E11 NL neurons tested (Fig. 4*D*).

Developmental differences in glutamate clearance at NL synapses

Another important factor that contributes to the summation of synaptically driven postsynaptic potentials is the clearance of glutamate from the synaptic cleft. We investigated this in NL neurons with a non-selective competitive inhibitor DL-threo-β-benzyloxyaspartate (TBOA), which blocks both glial and neuronal glutamate uptake. In E19 NL neurons, 100 μM TBOA caused a significant increase in the time course of the isolated NMDA-R-mediated EPSC (Fig. 5*A*). We quantified this change by measuring the width of the NMDA-R-mediated EPSC following low-frequency afferent stimulation (0.1 Hz) at half-maximal amplitude. At E19, under control conditions, the average half-width was 39.28 ms $\pm$ 5.76 ms but increased to 232.6 $\pm$ 62.70 ms after bath application of TBOA ($P < 0.01$; Fig. 5*B*). In contrast, at E11 we observed little change in the time course of the isolated NMDA-R-mediated EPSCs when TBOA was bath applied (Fig. 5*C*). Under control conditions and with bath application of TBOA, the average half-widths of the NMDA-R current response were 164.3 ms $\pm$ 22.54 ms and 177.8 $\pm$ 9.81, respectively ($P = 0.24$; Fig. 5*D*), suggesting a lack of transporter-mediated clearance of glutamate at NL synapses for E11 neurons.

These results indicate that at E11, the summation of EPSPs following rapid afferent stimulation and the subsequent ATDP is due to the summation of NMDA-R responses. These responses summate because of the slower kinetics of the GluN2B-containing NMDARs present at this age and because of an inefficient clearance of transmitter.

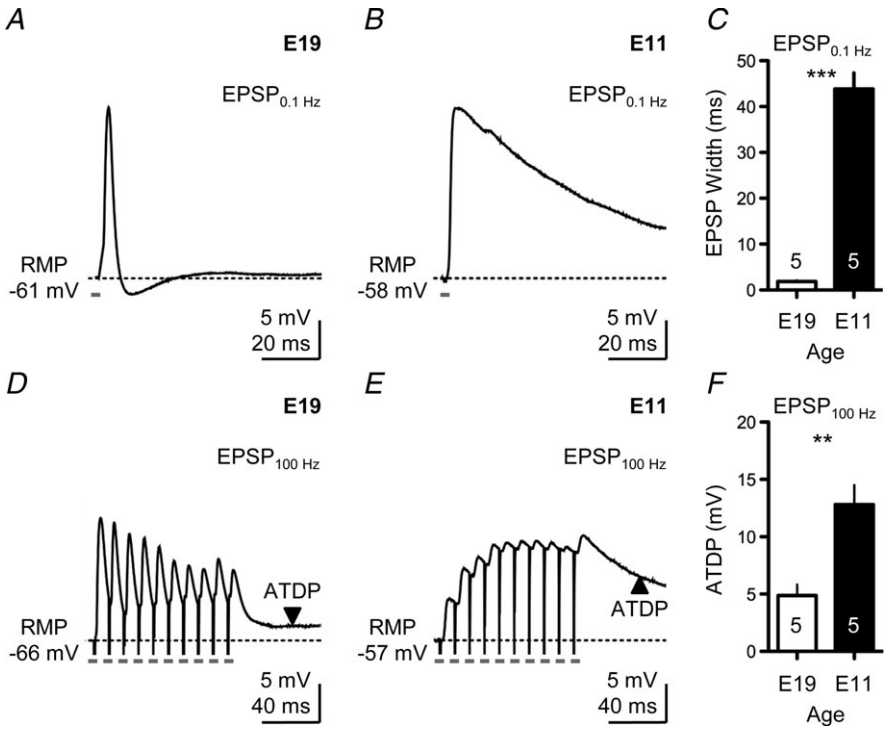

Figure 3. Developmental differences in excitatory postsynaptic potentials (EPSPs) following afferent stimulation
A, representative current-clamp trace showing the EPSP of an E19 NL neuron following low-frequency stimulation (0.1 Hz). *B*, representative current-clamp trace showing the EPSP of an E11 NL neuron following low-frequency stimulation (0.1 Hz). *C*, population data showing changes in the width of EPSPs measured at half-maximal amplitude for E19 and E11 NL neurons following low-frequency stimulation (0.1 Hz). *D*, representative current-clamp trace showing the EPSP of an E19 NL neuron elicited by a train of 10 pulses delivered at a rate of 100 Hz. Pulse train repeated every 10 s. *E*, representative current-clamp trace showing the EPSP of an E11 NL neuron elicited by a train of 10 pulses delivered at a rate of 100 Hz. Pulse train repeated every 10 s. *F*, population data showing changes in ATDP for E19 and E11 NL neurons following high-frequency stimulation (100 Hz). In *A*, *B*, *D* and *E*, traces are averaged across a minimum of 5 stimulus presentations. Stimulus intensity was adjusted to half the strength needed to elicit an AP, followed by TTX bath application.

Neuronal excitability is controlled by NMDA-Rs in developing NL neurons

We hypothesized that the strong depolarization mediated by NMDA-Rs controls the excitability of NL neurons via inactivation of Na^+ channels, thereby preventing repetitive AP generation during a rapid train of afferent stimulation. To assess this possibility, we blocked NMDA-Rs while recording the generation of APs during a train of rapid afferent stimulation from E19 and E11 NL neurons.

Ten pulses were delivered at a rate of 100 Hz and repeated once every 10 s. Figure 6*A* shows the response of an E19 NL neuron before (black trace) and after (red trace) bath application of DL-APV (100 μM), an NMDA-R antagonist. The overall neuronal excitability, the resting membrane potential or the number of APs generated during the stimulus train was not affected by APV (Fig. 6*A*–*D*). The probability of an AP occurring when NMDA-Rs were blocked did not change during any segment of the stimulus train, a result consistent for the population of E19 NL neurons tested (Fig. 6*B*, $n = 7$). Although blocking NMDA-Rs significantly reduced the ATDP across all neurons tested (Fig. 6*C*, $P < 0.01$) there were not changes in the RMP (Fig. 6*D*).

In contrast to the results obtained at E19, blocking NMDA-Rs with DL-APV at E11 resulted in the generation of APs that were able to follow the train of rapid afferent stimulation (Fig. 6*E*). In the control condition (no drug) the first two stimulus pulses in the train resulted in the generation of one AP and occasionally a second, while blocking NMDA-Rs (+APV) yielded APs that reliably responded during the entire stimulus train (10 APs, superimposed red trace). The probability of an AP occurring during the later segment of the stimulus train

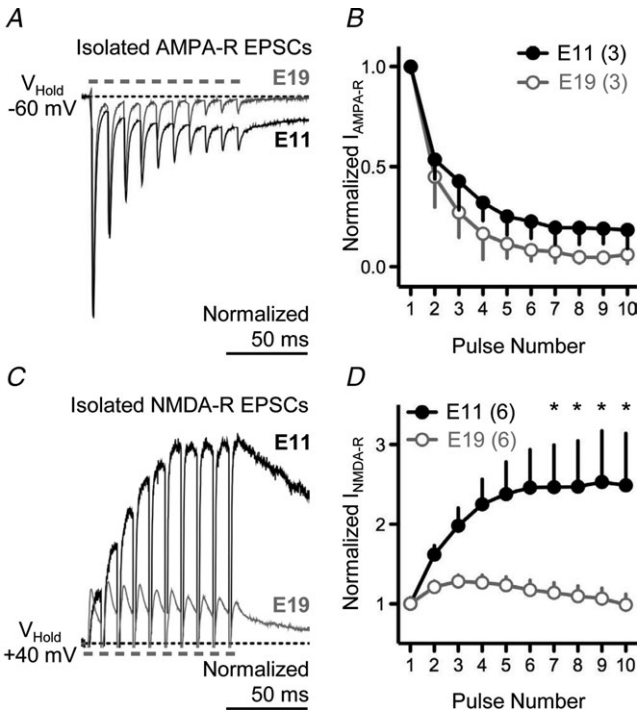

Figure 4. Developmental differences in excitatory postsynaptic currents (EPSCs) following rapid afferent stimulation
A, superimposed voltage-clamp traces of isolated AMPA-R-mediated EPSCs for E19 (grey trace) and E11 (black trace) NL neurons elicited by a train of 10 pulses delivered at a rate of 100 Hz. Pulse train repeated every 10 s. *B*, population data for isolated AMPA-R-mediated EPSCs for E19 and E11 NL neurons. *C*, superimposed voltage-clamp traces of isolated NMDA-R-mediated EPSCs for E19 (grey trace) and E11 (black trace) NL neurons elicited by a train of 10 pulses delivered at a rate of 100 Hz. Pulse train repeated every 10 s. *D*, population data for isolated NMDA-R-mediated EPSCs for E19 and E11 NL neurons. In *A* and *C*, traces are averaged across a minimum of 5 stimulus presentations.

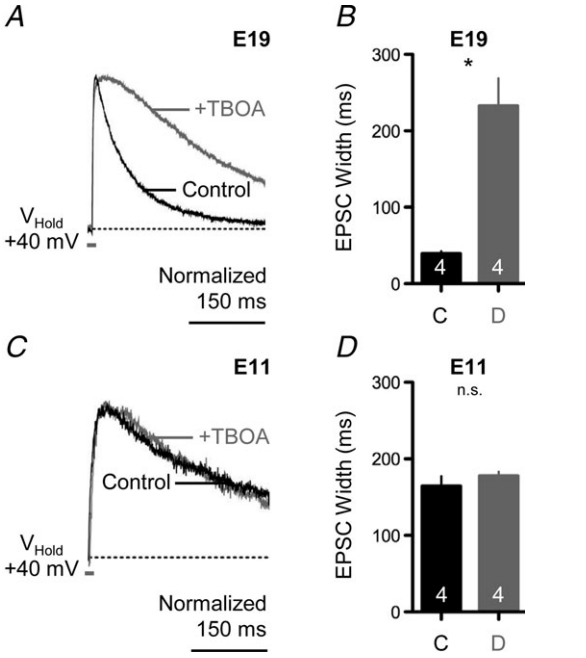

Figure 5. Developmental differences in glutamate clearance at NL synapses
A, representative voltage-clamp traces of isolated NMDA-R-mediated EPSCs for an E19 NL neuron before (black traces) and after (superimposed grey traces) bath application of a glutamate transporter antagonist (+TBOA, 100 μM). Afferent stimulation rate, 0.1 Hz. *B*, population data showing changes in the time to half-maximal amplitude width of the NMDA-R-mediated EPSC before (C, control) and during (D, drug) bath application of TBOA for E19 NL neurons. *C*, representative voltage-clamp traces of isolated NMDA-R-mediated EPSCs for an E11 NL neuron before (black traces) and after (superimposed grey traces) bath application of a glutamate transporter antagonist (+TBOA, 100 μM). Afferent stimulation rate, 0.1 Hz. *D*, population data showing changes in the time to half-maximal amplitude width of the NMDA-R-mediated EPSC before (C, control) and during (D, drug) bath application of TBOA for E11 NL neurons. In *A* and *C*, traces are averaged across a minimum of 5 stimulus presentations. In *B* and *D*, number in bar represents *n*. In this and subsequent figure, n.s., not significant.

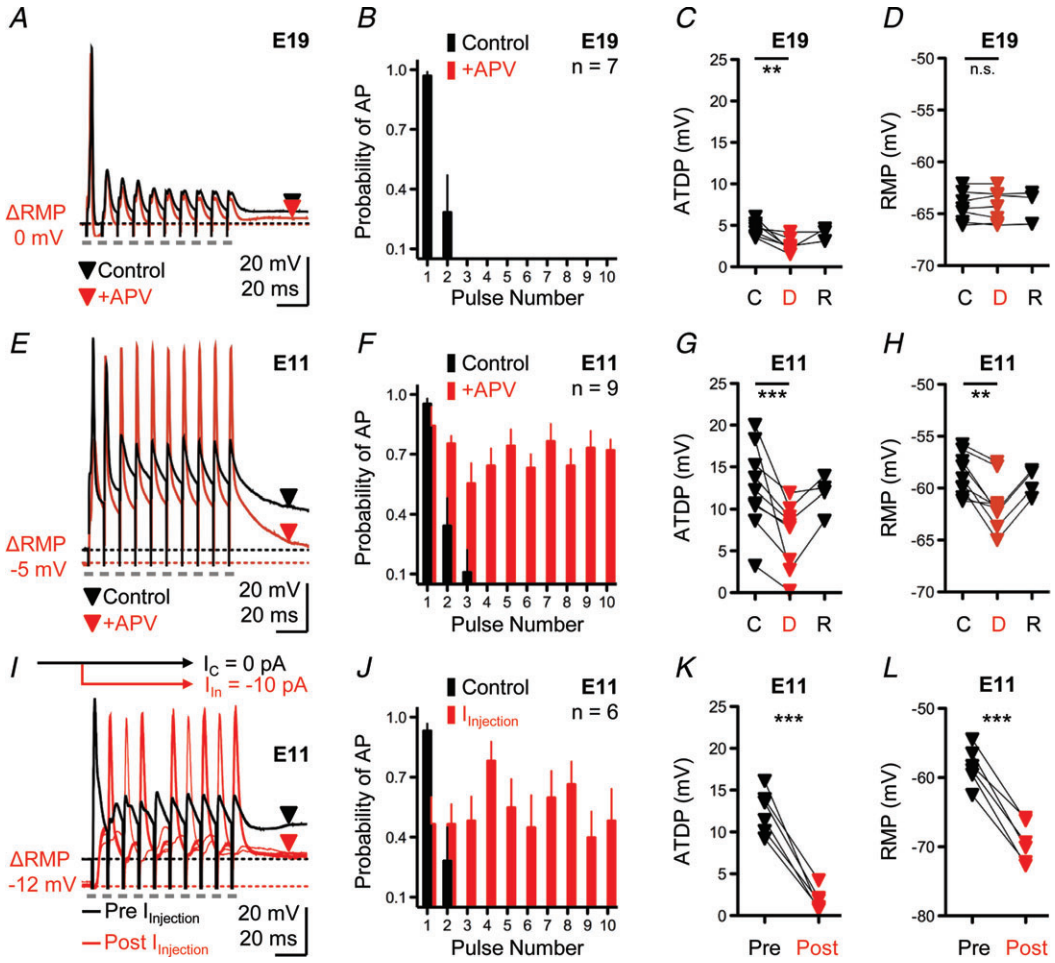

Figure 6. Neuronal excitability is controlled by NMDA-Rs in early developing NL neurons
A, representative current-clamp traces for an E19 NL neuron before (black traces) and after (superimposed red traces) bath application of an NMDA-R antagonist (+DL-APV, 100 μM). Stimulation, 10 pulses at a rate of 100 Hz, repeated every 10 s. ΔRMP is the change in resting membrane potential after application of DL-APV used to derive data shown in *D*. Black and red downward arrowheads (control and drug traces, respectively) represent time points (averaged across 10 ms window) used to derive data shown in *C*. *B*, population data for E19 NL neurons showing the probability of action potential occurrence as a function of pulse number during a 100 Hz train before (Control, black bars) and after (+APV, red bars) drug application. *C*, population data showing changes in ATDP before (C, control), during (D, drug) and after (R, recovery) bath application of DL-APV for E19 NL neurons. *D*, population data showing changes in RMP before (C), during (D) and after (R) bath application of DL-APV for E19 NL neurons. *E*, representative current-clamp traces for an E11 NL neuron before (black traces) and after (superimposed red traces) bath application of an NMDA-R antagonist (+DL-APV, 100 μM). Stimulation, 10 pulses at a rate of 100 Hz, repeated every 10 s. ΔRMP, change in resting membrane potential after application of DL-APV used to derive data shown in *H*. Black and red downward arrowheads (control and drug traces, respectively) represent time points (averaged across 10 ms window) used to derive data shown in *G*. *F*, population data for E11 NL neurons showing the probability of action potential occurrence as a function of pulse number during a 100 Hz train before (Control, black bars) and after (+APV, red bars) drug application. *G*, population data showing changes in ATDP before (C), during (D) and after (R) bath application of DL-APV for E11 NL neurons. *H*, population data showing changes in RMP before (C), during (D) and after (R) bath application of DL-APV for E11 NL neurons. *I*, representative traces for an E11 NL neurons before (Pre $I_{Injection}$, black trace) and after (Post $I_{Injection}$, red traces) somatic current injection. Black schematic line with arrow shown above traces represents control holding current ($I_C = 0$ pA). Red schematic line with arrow shown above traces represents hyperpolarizing current injected into soma ($I_{In} = -10$ pA). ΔRMP, change in resting membrane potential after somatic injection of a hyperpolarizing current. Black and red downward arrowheads (control and current injection traces, respectively) represent time points (averaged across 10 ms window) used to derive data shown in *K*. *J*, population data for E11 NL neurons showing the probability of action potential occurrence as a function of pulse number during a 100 Hz train before (Control, black bars) and after ($I_{Injection}$, red bars) somatic current injection. *K*, population data showing changes in ATDP before (Pre) and during (Post) hyperpolarizing somatic current injections for E11 NL neurons. *L*, population data showing changes in RMP before (Pre) and during (Post) hyperpolarizing somatic current injections for E11 NL neurons. Recovery traces in *A*, *E* and *I* not shown for clarity.

was consistent across all E11 NL neurons sampled when NMDA-Rs were blocked with DL-APV (Fig. 6*F*, $n = 9$). For the neuron in Fig. 6*E*, the ATDP plateau, measured 50 ms after the final pulse in the train (red triangle), was 18.3 mV in the control condition but was reduced to 2.7 mV following blockade of NMDA-Rs. In all E11 NL neurons tested, blocking NMDA-Rs resulted in a 44% reduction in the ATDP ($P < 0.001$, Fig. 6*G*). Surprisingly, we also observed a significant change in the RMP following bath application of DL-APV at E11 ($P < 0.01$). This change in the RMP was always hyperpolarizing, averaging -58.78 ± 2.01 mV in the control condition and -64.03 ± 1.47 mV following DL-APV application (Fig. 6*H*).

These results indicate that at an age when K_{LVA} are underdeveloped, NMDA-Rs control the output of NL neurons through their ability to summate EPSPs and the inefficient clearance of transmitter, a combination that produces a sustained depolarization that presumably maintains Na^+ channels in an inactivated state. To test this, we hyperpolarized E11 NL neurons in an attempt to recover Na^+ channels from inactivation while synaptically stimulating afferent inputs with a train of pulses (10 pulses at a rate of 100 Hz). A representative example of an E11 NL neuron is shown in Fig. 6*I*. Prior to somatic current injection, the average resting membrane potential was -54.47 mV and the ATDP was 10.21 mV. Rapid afferent stimulation resulted in the generation of a single AP (black trace), similar to results shown previously (Figs 1*C* and 6*E*). After injection of a steady-state hyperpolarizing current into the soma (10 pA), the neuron hyperpolarized to -66.19 mV and the ATDP was reduced to $\sim$1 mV. This amount of hyperpolarization allowed the neuron to reliably generate APs during the later segment of the train of pulses (8 APs, superimposed red traces), presumably due to recovery of available Na^+ channels from inactivation. In addition, we found that E11 NL neurons were able to generate an AP as early as 100 ms following the last stimulus pulse in the train (data not shown), suggesting that in normal conditions, the time interval between spontaneous bursts of activity reported previously ($\sim$4 s, Lippe, 1994) provides ample amount of time for Na^+ channels to reactivate and contribute to AP generation.

The probability of an AP occurring during somatic current injection was consistent across the sample of E11 NL neurons tested (Fig. 6*J*, $n = 6$). For all neurons tested, somatic current injection ranging from 5 to 13 pA significantly reduced the ATDP ($P < 0.001$, Fig. 6*K*). The average RMP before current injection was -58.41 mV (± 2.73 mV); steady-state somatic current injection hyperpolarized the cell on average to -69.43 mV (± 2.92 mV; $P < 0.001$, Fig. 6*L*).

These results indicate that the summation of NMDA-R-mediated EPSPs following rapid afferent stimulation depolarize the membrane, keeping Na^+ channels in an inactive state. This effect is sufficient to filter the output of NL neurons before intrinsic properties are completely developed.

It is of interest to highlight the change in RMP to hyperpolarizing values in E11 NL neurons after application of the NMDA-R antagonist DL-APV. This suggests the presence of a constant NMDA-R-mediated current presumably due to a larger concentration of extracellular glutamate. Is it possible that GluN2B-containing NMDA-Rs, while controlling neuronal excitability for incoming synaptic activity, are constantly activated by ambient glutamate? More importantly, why does this constant activation of NMDA-Rs not generate an increase in spontaneous AP firing at this age?

Developmental differences in current–voltage (*I–V*) curves of isolated NMDA-R-mediated EPSCs

External Mg^{2+} blocks NMDA-Rs near resting membrane potentials in most neurons (Traynelis *et al.* 2010). However, it is conceivable that developmental differences in the sensitivity to external Mg^{2+} could provide an additional mechanism contributing to constant NMDA-R activation near the RMP of early developing NL neurons. To address this, we recorded isolated NMDA-R-mediated EPSCs while voltage-clamping NL neurons at different holding potentials during low-frequency afferent stimulation (0.1 Hz). A representative recording from an E19 NL neuron is shown in Fig. 7*A*. The isolated NMDA-R-mediated EPSC resulted in both inward and outward responses when the neuron was voltage-clamped from -90 mV to $+40$ mV, respectively (in steps of 5–10 mV). For this particular neuron, the maximum inward current was recorded when the neuron was voltage-clamped at -20 mV ($I_{NMDA} = -52.8$ pA). Similar to E19, isolated NMDA-R-mediated EPSCs from E11 NL neurons resulted in both inward and outward responses when the neuron was voltage-clamped from -90 mV to $+40$ mV. A representative recording is shown in Fig. 7*B*. For this E11 neuron, however, the maximum inward current was recorded when the neuron was voltage-clamped at -40 mV ($I_{NMDA} = -101.1$ pA), suggesting weaker sensitivity to external Mg^{2+} blockade. Data for a group of neurons at each age are shown in Fig. 7*C* and *D*.

The maximum inward current (when normalized to the maximum outward current mediated at $+40$ mV) at E11 was observed at less depolarizing voltage commands compared with E19 responses (Fig. 7*C*). In E11 neurons, strong isolated NMDA-R-mediated EPSCs were evident at holding potentials just 5–10 mV above the average RMP, and the current generated at -50 mV was twice as large as currents recorded at E19 (Fig. 7*D*; absolute I_{NMDA}

at −50 mV = −96.3 ± 27.4 pA and −41.1 ± 15.9 for E11 and E19, respectively, $n = 4$ each). Taken together, the results indicate that developmental differences in external Mg^{2+} sensitivity (Fig. 7) and a lack of glutamate clearance (Fig. 5) could account for changes in the RMP observed at E11 after NMDA-R blockade (Fig. 6*H*).

Developmental differences in the site of expression of low-voltage-activated K^+ channels

If there is constant activation of NMDA-Rs at E11, why does this depolarization not generate a positive feedback, eventually triggering spontaneous APs? We suspected that the small conductance of K_{LVA} channels that are activated just above RMP (see Fig. 2) is sufficient to prevent run-away depolarization. Therefore, we asked if K_{LVA}-containing channels are differentially localized in E19 and E11 NL neurons.

Immunolabelling of Kv1.2 in E19 NL slices shows modest labelling in the somatic and dendritic regions of NL, consistent with previous reports (Kuba *et al.* 2005). Strong immunoreactivity can be observed concentrated on a projection near the soma, presumably the proximal axon (Fig. 8*A*). Interestingly, the expression of Kv1.2 channels shows a different distribution at E11. Kv1.2 expression at E11 appears strong on somatic and dendritic regions of NL and the pattern of labelling appears to be more punctate when compared with E19 tissue (Fig. 8*B*).

To evaluate the expression pattern across several cell layers, we prepared optical density intensity profiles of Kv1.2 immunoreactivity across entire 35 μm tissue sections. Again, at E19 the amount of label intensity is modest across dendritic and somatic regions in NL, but strong Kv1.2 expression on the ventrally projecting

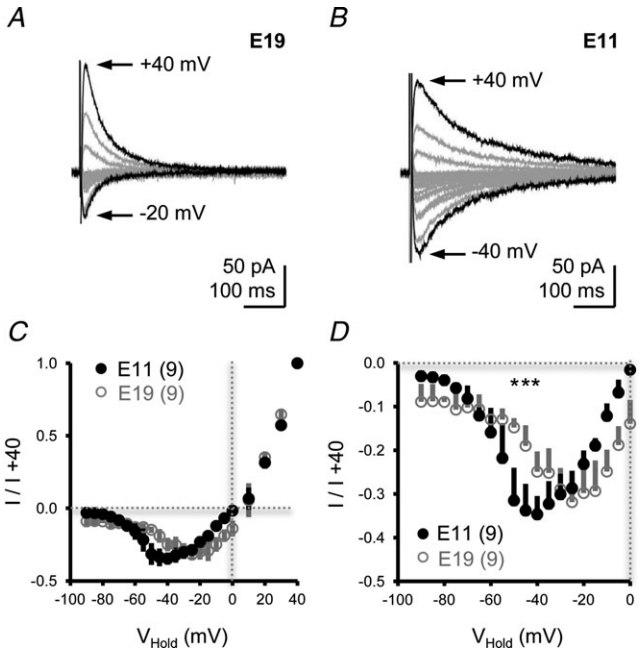

Figure 7. Developmental differences in current–voltage (*I–V*) curves of isolated NMDA-R-mediated EPSCs
A and *B*, representative voltage-clamp traces of isolated NMDA-R-mediated EPSCs for E19 (*A*) and E11 (*B*) NL neurons. Neurons were voltage-clamped from −90 mV to +40 mV (steps of 5–10 mV). Black traces in *A* and *B* show maximum EPSCs at hyperpolarizing (E19, −20 mV; E11, −40 mV) and depolarizing (E19 and E11, +40 mV) holding potentials. Afferent stimulation rate, 0.1 Hz. Traces are averaged across a minimum of 5 stimulus presentations. *C*, population *I–V* curves for E19 and E11 NL neurons normalized to the isolated NMDA-mediated EPSC recorded at +40 mV. *D*, close-up of population *I–V* curves shown in *C* at holding voltages between −90 mV and 0 mV.

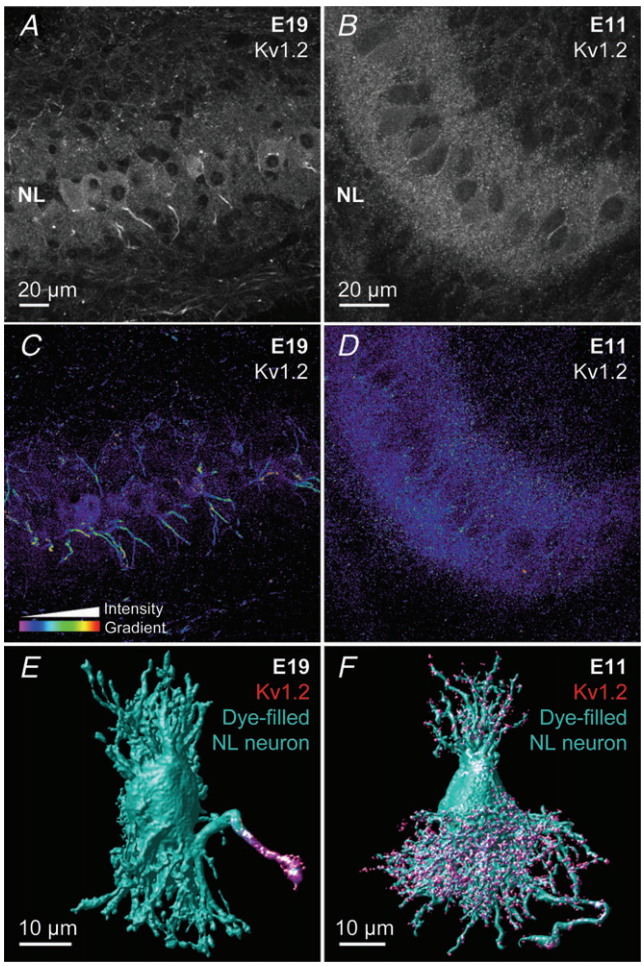

Figure 8. Developmental differences in the expression of low-voltage-activated K^+ channels
A and *B*, projection images (10 optical sections, 0.3 μm each) showing anti-Kv1.2 immunoreactivity at E19 (*A*) and E11 (*B*) in NL. *C* and *D*, intensity profile of optical density for the same tissue sample shown in *A* and *B*. 3-D image stack was taken throughout the entire 35 μm sections and shows Kv1.2 expression in NL over several cell layers of E19 (*C*) and E11 (*D*). *E* and *F*, single cell electroporation combined with immunohistochemistry showing Kv1.2 expression predominantly on the proximal axon at E19 (*E*) and on dendrites at E11 (*F*).

NL axons is present throughout the entire tissue section (Fig. 8*C*). In contrast, Kv1.2 at E11 is strongly expressed in the dendritic region of NL neurons, with comparable labelling around the somatic layer (Fig. 8*D*). Over several cell layers (35 μm sections), no centralized Kv1.2 immunostaining appears present on the proximal axon.

To confirm that the concentrated expression pattern of Kv1.2 is indeed localized to the proximal axon at E19 and dendritic region at E11, we combined Kv1.2 immunoreactivity with single-cell electroporation of a fluorescent dye to 3-D reconstruct individual neurons. Figure 8*E* shows that at E19, Kv1.2 labelling is strongly concentrated in the proximal axon. In contrast at E11, Kv1.2 labelling is primarily dendritic (Fig. 8*F*) and again does not reveal a comparable level of Kv1.2 expression on the proximal axon.

We could not obtain reliable immunostaining for Kv1.1, the other K_{LVA} channel known to be present in mature NL neurons (Lu *et al.* 2004; Kuba *et al.* 2005). Furthermore, we could not rule out the possibility of presynaptic labelling of Kv1.2 channels at E11. Future studies are needed to determine the specific location of Kv1.2 channels in NL at this developmental time period. Our electrophysiological data, however, indicate that ~33% of the total K^+ current measured between −55 mV and −30 mV is sensitive to bath application of DTx-I, a K_{LVA} channel blocker (Fig. 2), suggesting that some K^+ current is mediated by channels located on NL neurons. Despite a relatively small presence of K_{LVA} channels at E11, dendritic localization of at least one sub-family member (Kv1.2) could prevent run-away depolarization due to tonic activation of NMDA-Rs at this age.

Low-voltage-activated K^+ channels prevent NMDA-R-mediated run-away depolarization

To test whether the dendritic expression pattern and small conductance of K_{LVA} is sufficient to prevent run-away depolarization of E11 NL neurons, we recorded spontaneous changes in postsynaptic membrane potential during multiple conditions. Spontaneous events were recorded in current-clamp mode for a minimal period of 5 min in control conditions, or after the addition of DTx or APV.

In the control condition for the E11 NL neuron shown in Fig. 9*A* left panel, no spontaneous APs were recorded during the 5 min time window, only small positive deflections in the membrane potential were infrequently observed (presumably spontaneous EPSPs). However, bath application of the K_{LVA} channel blocker DTx-I (0.1 μM), increased brief periods of membrane depolarizations by tens of millivolts. During these depolarizing periods, occasional bursts of spontaneous APs were generated (Fig. 9*A*, centre panel), presumably because the depolarization was sufficient in magnitude to reach AP threshold. Additional bath application of the NMDA-R antagonist DL-APV eliminated most of the APs generated during these depolarized periods (Fig. 9*A*, right panel). Thus, E11 NL neurons exhibit extremely low spontaneous activity as measured by AP generation. Blocking K_{LVA} channels with DTx-I increased the spontaneous generation of APs in 5 of 11 NL neurons (Fig. 9*B*) with no change in the RMP ($P = 0.45$; Fig. 9*C*). In six NL neurons, addition of DTx increased fluctuations in the membrane potential but no APs were generated. Subsequent bath application of the NMDA-R antagonist DL-APV significantly reduced the generation of spontaneous APs ($P < 0.01$; Fig. 9*B*) and hyperpolarized neurons by ~10 mV ($P < 0.01$; Fig. 9*C*), as observed before (Fig. 6*H*).

Taken together, these results indicate that under basal spontaneous activity in the slice, NMDA-Rs are constantly activated at E11, presumably due to an inadequate clearance of transmitter from the synapse and a reduced

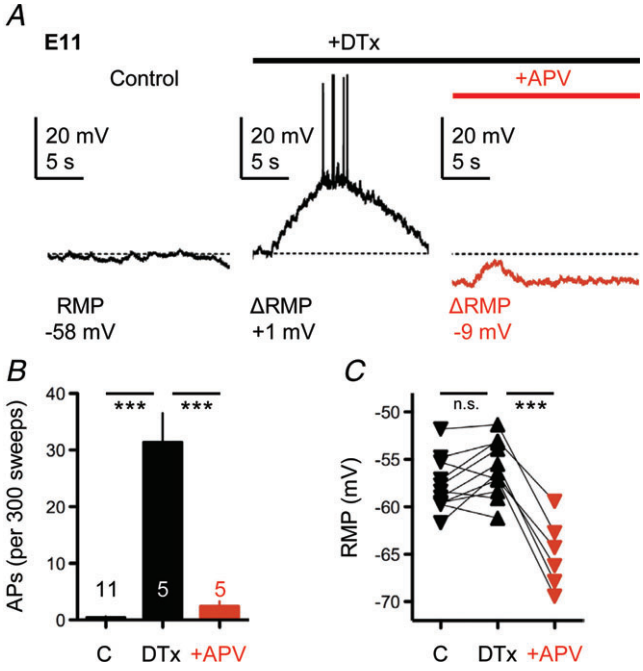

Figure 9. Low-voltage-activated K^+ channels prevent NMDA-R-mediated run-away depolarization
A, representative current-clamp traces (20 s windows) from an individual E11 NL neuron showing changes in spontaneous membrane voltages between control condition (left, black trace), DTx-I application (0.1 μM, middle, black trace) and subsequent DL-APV application (100 μM, right, red trace). Bars above traces represent relative time course of drug application (black bar, +DTx-I; red bar, +DL-APV). Baseline RMP (dashed line) and changes in RMP (ΔRMP) after drug applications are shown. *B*, population data showing changes in the generation of spontaneous APs during the different recording conditions (C, control; DTx, K_{LVA} block; +APV, NMDA-R block). *C*, population data showing changes in the baseline RMP during the different recording conditions.

sensitivity of GluN2B-containing NMDA-Rs to exogenous Mg^{2+} blockade. This constant activation of NMDA-Rs results in increased neuronal excitability in NL that is able to contribute to the generation of spontaneous APs. However, K_{LVA}, localized in dendritic and somatic areas, may help prevent run-away NMDA-R activation.

Discussion

We show that early in development, NL neurons respond with one or two initial APs to repetitive synaptic stimulation on one side of the brainstem, similar to what has been described in mature-like NL neurons (Kuba *et al.* 2002). During this early developmental time period synaptic NMDA-type glutamate receptors (NMDA-Rs) contain primarily the GluN2B subunit (Sanchez *et al.* 2010). This subunit composition of the NMDA-R allows synaptic responses to summate, filtering the output of NL neurons before intrinsic properties are fully developed. Weaker Mg^{2+} blockade of NMDA-Rs and ambient glutamate generate a tonic NMDA-R-mediated current that sets the membrane potential at more depolarized values. Small K_{LVA} conductances localized in dendrites prevent excessive depolarization caused by tonic activation of NMDA-Rs. Thus, before intrinsic properties are fully developed, NMDA-Rs control the output of NL neurons during evoked synaptic transmission.

The mechanisms and importance of this highly filtered neuronal output in mature-like auditory neurons is well understood in birds and mammals (for reviews see Oertel, 1991, 1997; Trussell, 1998, 1999; Burger & Rubel, 2008; Kuba, 2010). In mature-like auditory neurons, control of neuronal excitability is critical for optimizing converging inputs and to accurately ensure that phase-locked information is preserved (Oertel, 1991, 1997). Intrinsic and synaptic factors contribute to the regulation of neuronal excitability. Intrinsic factors include the site of axonal AP initiation (Kuba *et al.* 2006, 2010) and large K_{VA} conductances (Reyes *et al.* 1996; Kuba *et al.* 2003). Particularly important are K_{LVA} conductances that are activated just above the RMP (Gao & Lu, 2008). Their strong outward ion flux near the RMP increases AP threshold, reduces AP height and limits the time-course inputs can summate, all important biophysical properties required for detection of coincident synaptic inputs (Oertel, 1991, 1997; Reyes *et al.* 1994; Brew & Forsythe, 1995; Rothman & Manis, 2003; Barnes-Davies *et al.* 2004; Ashida *et al.* 2007; Howard & Rubel, 2010; Mathews *et al.* 2010). In addition, K_{HVA} conductances are activated after AP generation (~20 mV) (Gan & Kaczmarek, 1998) and allow rapid repolarization, preserving high-frequency firing in a phase-locked fashion (Brew & Forsythe, 1995; Wang *et al.* 1998; Gao & Lu, 2008).

Specialized synaptic properties also contribute to control neuronal excitability in mature auditory neurons. Some of these synaptic properties include: (1) the depletion of phasically released vesicles from presynaptic terminals (Kuba *et al.* 2002; Cook *et al.* 2003), (2) the efficient clearance of transmitter from synapses (Otis *et al.* 1996), (3) the rapid kinetics, desensitization and inward rectification of AMPA-Rs (Raman *et al.* 1994; Ravindranathan *et al.* 2000; Slee *et al.* 2010; Sanchez *et al.* 2010), and (4) the tonic activation of depolarizing GABAergic inputs (Tang *et al.* 2011). Thus, mature-like auditory neurons generate one or two initial APs in response to strong and repetitive ipsilateral synaptic stimulation or constant depolarizing inputs. To our surprise, before many intrinsic and synaptic properties are fully developed and before the onset of hearing, the output of NL neurons is filtered similarly to mature-like neurons, producing one or two initial APs in response to strong and rapid ipsilateral synaptic stimulation.

The importance of neuronal filtering in early developing auditory neurons is not well understood, despite evidence of such filtering at other developing central auditory synapses (Taschenberger & von Gersdorff, 2000; Futai *et al.* 2001). In NL, long-lasting EPSPs are able to summate due to the NMDA-R subunit composition and the weaker blockade by external Mg^{2+}. In addition, a lack of glutamate reuptake and Na^{+} channels inactivation assist NMDA-Rs in filtering NL output. The role of such filtering could be critical when considering the bilateral innervation these neurons receive. Long-lasting EPSPs could allow the summation of bilateral inputs to arrive within a specific time window, generating an AP only when appropriately timed inputs coincide, discarding other inputs that do not fall within this time window. It is tempting to speculate that this could be a selection process that assists in refining appropriate connections between NM and NL.

An interesting relationship between the early development of K^{+} channels conductances and the subunit contribution of synaptic NMDA-Rs exists in this circuit known for the control of AP output. Our data indicate that K_{VA} conductances are relatively small early in development during the synaptogenesis period (E11), with K_{LVA} channels accounting only for ~33% of the total K_{VA} conductance, similar to other reports (Kuba *et al.* 2002, 2005; Gao & Lu, 2008). Despite the fact that the density of K_{LVA} channels is lower early in development, its conductance could be substantial relative to the background leak conductance. Interestingly, the expression pattern of K_{LVA} containing the Kv1.2 subunit, one of the K_{LVA} subfamilies known to be present in mature NL neurons (Kuba *et al.* 2005), was primarily dendritic and somatic at E11, in contrast to the strong axonal expression at E19.

Although we cannot rule out the possibility that K_{LVA} channels expression is also partially presynaptic,

the presence of postsynaptic K_{LVA} channels and the fact that DL-APV immediately reverses the depolarizing ramps and APs observed in NL neurons (Fig. 9), suggest that the role of K_{LVA} is to prevent run-away excitation caused by tonic activation of NMDA-Rs. Other low-voltage-activated conductances insensitive to DTx-I present at E11 may not have the proper spatial distribution to efficiently suppress neuronal excitability driven by ambient glutamate and tonic NMDAR currents. It has been shown that a biased gradient of K^+ channel expression is found in the mammalian auditory brainstem responsible for encoding binaural inputs (for review see Johnston *et al.* 2010). The somatic bias of K_{LVA} channels compensates for passive cable filtering during propagation of EPSPs in dendrites by accelerating repolarization in a voltage-dependent manner, improving the time resolution of synaptic integration (Mathews *et al.* 2010). These results suggest that both the spatial distribution and voltage-dependent properties of K_{LVA} channels are essential for reducing excitability and may operate in a similar fashion in early developing NL by controlling excessive NMDA-R-dependent depolarization.

Synaptic properties during this early developmental period are also different. At E11, AMPA-R-mediated currents are slower and less rectifying (Sanchez *et al.* 2010) and the glutamate uptake system is underdeveloped or non-existing (this study). However, AMPA-R-mediated currents exhibit a strong depression after repetitive stimulation, similar to what is observed in mature-like neurons. Although AMPA-Rs are important for rapid and reliable initial depolarization, this suggests they contribute minimally to the control of neuronal excitability upon repetitive afferent stimulation.

Another important synaptic difference between young neurons (E11) and mature-like neurons (E19) is the subunit composition of NMDA-Rs. At E11, during the period of synaptogenesis in NL, NMDA-Rs contain primarily the GluN2B subunit that produces longer lasting EPSCs than the more mature GluN2A-containing NMDA-Rs observed at E19 (Sanchez *et al.* 2010). This developmental switch in subunit composition has been described for several brain regions (Yashiro & Philpot, 2008). The observed shift in the *I–V* relationship of synaptic NMDA-R responses could be attributed to differential Mg^{2+} sensitivity of GluN2B- and GluN2A-containing receptors or to a small contribution of GluN2C, a subunit less sensitive to Mg^{2+} blockade (Traynelis *et al.* 2010). This property, along with an underdeveloped glutamate re-uptake system, allows the summation of NMDA-R currents that cause a sustained after-train depolarization plateau. This sustained depolarization prevents the re-activation of Na^+ channels after a train of ipsilateral synaptic inputs triggers one or two initial APs. Thus, NMDA-Rs effectively control neuronal excitability early in development of NL neurons.

How NL neurons recover from Na^+ channel inactivation and generate APs is of particular interest because of the high firing rate of mature-like NM neurons (Born *et al.* 1991). The *in vivo* firing rate of NM neurons before hearing onset (<E14) is not known; however, spontaneous AP activity at E14–E15 has a mean inter-burst interval of 4.9 s that decreases to 2.1 s at E18. By E19, synchronous bursting is replaced by an unpatterned, steady level of firing (Lippe, 1994), comparable to the background discharge present in NM and NL of hatchling birds (Born *et al.* 1991). Thus, NL neurons could recover from Na^+ channel inactivation in a time- and voltage-dependent fashion between burst of spontaneous activity. Indeed, we found that E11 NL neurons were able to generate an AP as early as 100 ms following the last stimulus pulse in the train, suggesting that the time intervals between spontaneous bursts of activity reported previously (Lippe, 1994) provide ample amount of time for Na^+ channels to reactivate and contribute to AP generation.

Lack of glutamate uptake causes an increase in ambient glutamate and a tonic activation of NMDA-Rs as revealed by a drop in the RMP upon blockade of NMDA-Rs. This constant activation is possible because of the GluN2B subunit composition of NMDA-Rs that have a high affinity for glutamate (Patneau & Mayer, 1990) and lower sensitivity to exogenous Mg^{2+} blockade than the mature form of NMDA-Rs (this study). Activation of a small number of GluN2B-containing receptors could rapidly generate a positive feedback because the pronounced negative slope observed in the *I–V* curve of NMDA-Rs responses at E11. Early in development, because of the constant presence of glutamate, NMDA-Rs act as a voltage-activated channel able to produce a significant depolarization of the membrane. However, we report here that the small K_{LVA} conductances prevent excessive depolarization and hyperexcitability of NL neurons.

As the circuit develops, functional K_{LVA} channels are up-regulated (Gao & Lu, 2008), their expression pattern becomes more axonal (this study), and NMDA-Rs change subunit content (Sanchez *et al.* 2010). Although there are synaptic responses mediated by NMDA-R at E19 in NL (Sanchez *et al.* 2010; this study), their functional contribution to neuronal excitability is minimal. This is presumably due to the subunit composition of NMDA-Rs late in development (i.e. predominately GluN2A-containing), the speeding of their kinetics and an effective glutamate uptake system. It remains to be determined what synaptic role GluN2A-containing NMDA-Rs play late in NL development. It is possible, however, that the developmental down-regulation of NMDA-Rs and the change in their subunit content is necessary for normal synaptic maturation to occur in NL, as seen in other central synapses (Taschenberger & von Gersdorff, 2000; Futai *et al.* 2001; Gambrill *et al.* 2011).

Before intrinsic properties are fully developed, NMDA-Rs control the output of NL neurons during evoked synaptic transmission while K_{LVA} play a role in counteracting the tonic activity of NMDA-Rs. We suggest that this interaction between NMDA-Rs and K_{LVA} during development contributes to filter the output of NL neurons. This pre-hearing filtering of NL responses presumably plays a different role than in the mature hearing system. Synaptic responses mediated by GluN2B-containing NMDA-Rs may be required for sculpting NL specializations that are important for mature time-coding binaural auditory neurons while the filtering of neuronal output may assist in the selection of appropriated synapses and circuit refinement.

References

Ashida G, Abe K, Funabiki K & Konishi M (2007). Passive soma facilitates submillisecond coincidence detection in the owl's auditory system. *J Neurophysiol* **97**, 2267–2282.

Barnes-Davies M, Barker MC, Osmani F & Forsythe ID (2004). Kv1 currents mediate a gradient of principal neuron excitability across the tonotopic axis in the rat lateral superior olive. *Eur J Neurosci* **19**, 325–333.

Bartlett EL & Smith PH (2002). Effects of paired-pulse and repetitive stimulation on neurons in the rat medial geniculate body. *Neuroscience* **113**, 957–974.

Born DE, Durham D & Rubel EW (1991). Afferent influences on brainstem auditory nuclei of the chick: nucleus magnocellularis neuronal activity following cochlea removal. *Brain Res* **557**, 37–47.

Brew HM & Forsythe ID (1995). Two voltage-dependent K^+ conductances with complementary functions in postsynaptic integration at a central auditory synapse. *J Neurosci* **15**, 8011–8022.

Burger RM & Rubel EW (2008). Encoding of interaural timing for binaural hearing. In *The Senses: A Comprehensive Review*, vol. 3, *Audition*, ed. Dallos P & Oertel D, pp. 613–630. Academic Press, San Diego.

Burnashev N, Zhou Z, Neher E & Sakmann B (1995). Fractional calcium currents through recombinant GluR channels of the NMDA, AMPA and kainate receptor subtypes. *J Physiol* **485**, 403–418.

Carr CE & Konishi M (1990). A circuit for detection of interaural time differences in the brain stem of the barn owl. *J Neurosci* **10**, 3227–3246.

Cook DL, Schwindt PC, Grande LA & Spain WJ (2003). Synaptic depression in the localization of sound. *Nature* **421**, 66–70.

Erreger K, Dravid SM, Banke TG, Wyllie DJ & Traynelis SF (2005). Subunit-specific gating controls rat NR1/NR2A and NR1/NR2B NMDA channel kinetics and synaptic signaling profiles. *J Physiol* **563**, 345–358.

Flint AC, Maisch US, Weishaupt JH, Kriegstein AR & Monyer H (1997). NR2A subunit expression shortens NMDA receptor synaptic currents in developing neocortex. *J Neurosci* **17**, 2469–2476.

Futai K, Okada M, Matsuyama K & Takahashi T (2001). High-fidelity transmission acquired via a developmental decrease in NMDA receptor expression at an auditory synapse. *J Neurosci* **21**, 3342–3349.

Gambrill AC, Storey GP & Barria A (2011). Dynamic regulation of NMDA receptor transmission. *J Neurophysiol* **105**, 162–171.

Gan L & Kaczmarek LK (1998). When, where, and how much? Expression of the Kv3.1 potassium channel in high-frequency firing neurons. *J Neurobiol* **37**, 69–79.

Gao H & Lu Y (2008). Early development of intrinsic and synaptic properties of chicken nucleus laminaris neurons. *Neuroscience* **153**, 131–143.

Hestrin S (1992). Developmental regulation of NMDA receptor-mediated synaptic currents at a central synapse. *Nature* **357**, 686–689.

Hogsden JL & Dringenberg HC (2009). NR2B subunit-dependent long-term potentiation enhancement in the rat cortical auditory system *in vivo* following masking of patterned auditory input by white noise exposure during early postnatal life. *Eur J Neurosci* **30**, 376–384.

Howard MA & Rubel EW (2010). Dynamic spike thresholds during synaptic integration preserve and enhance temporal response properties in the avian cochlear nucleus. *J Neurosci* **30**, 12063–12074.

Johnston J, Forsythe ID & Kopp-Scheinpflug C (2010). Going native: voltage-gated potassium channels controlling neuronal excitability. *J Physiol* **588**, 3187–3200.

Joseph AW & Hyson RL (1993). Coincidence detection by binaural neurons in the chick brain stem. *J Neurophysiol* **69**, 1197–1211.

Kuba H (2010). Plasticity at the axon initial segment. *Commun Intgr Biol* **6**, 597–598.

Kuba H, Ishii TM & Ohmori H (2006). Axonal site of spike initiation enhances auditory coincidence detection. *Nature* **444**, 1069–1072.

Kuba H, Koyano K & Ohmori H (2002). Synaptic depression improves coincidence detection in the nucleus laminaris in brainstem slices of the chick embryo. *Eur J Neurosci* **15**, 984–990.

Kuba H, Oichi Y & Ohmori H (2010). Presynaptic activity regulates Na^+ channel distribution at the axon initial segment. *Nature* **465**, 1075–1078.

Kuba H, Yamada R, Fukui I & Ohmori H (2005). Tonotopic specialization of auditory coincidence detection in nucleus laminaris of the chick. *J Neurosci* **25**, 1924–1934.

Kuba H, Yamada R & Ohmori H (2003). Evaluation of the limiting acuity of coincidence detection in nucleus laminaris of the chicken. *J Physiol* **552**, 611–620.

Lippe WR (1994). Rhythmic spontaneous activity in the developing auditory brainstem. *J Neurosci* **3**, 1486–1495.

Lu Y, Harris JA & Rubel EW (2007). Development of spontaneous miniature EPSCs in mouse AVCN neurons during a critical period of afferent-dependent neuron survival. *J Neurophysiol* **97**, 635–646.

Lu Y, Monsivais P, Tempel BL & Rubel EW (2004). Activity-dependent regulation of the potassium channel subunits Kv1.1 and Kv3.1. *J Comp Neurol* **470**, 93–106.

Mathews PJ, Jercog PE, Rinzel J, Scott LL & Golding NL (2010). Control of submillisecond synaptic timing in binaural coincidence detectors by K_v1 channels. *Nat Neurosci* **13**, 601–609.

Oertel D (1991). The role of intrinsic neuronal properties in the encoding of auditory information in the cochlear nuclei. *Curr Opin Neurobiol* **1**, 221–228.

Oertel D (1997). Encoding of timing in the brain stem auditory nuclei of vertebrates. *Neuron* **19**, 959–962.

Otis TS, Wu YC & Trussell LO (1996). Delayed clearance of transmitter and the role of glutamate transporters at synapses with multiple release sites. *J Neurosci* **16**, 1634–1644.

Parameshwaran-Iyer S, Carr CE & Perney TM (2003). Localization of KCNC1 (Kv3.1) potassium channel subunits in the avian auditory nucleus magnocellularis and nucleus laminaris during development. *J Neurobiol* **55**, 165–178.

Patneau DK & Mayer ML (1990). Structure-activity relationships for amino acid transmitter candidates acting at N-methyl-D-aspartate and quisqualate receptors. *J Neurosci* **10**, 2385–2399.

Pena JL, Viete S, Funabiki K, Saberi K & Konishi M (2001). Cochlear and neural delays for coincidence detection in owls. *J Neurosci* **21**, 9455–9459.

Pliss L, Yang H & Xu-Friedman MA (2009). Context-dependent effects of NMDA receptors on precise timing information at the endbulb of held in the cochlear nucleus. *J Neurophysiol* **102**, 2627–2637.

Porres CP, Meyer EM, Grothe B & Felmy F (2011). NMDA currents modulate the synaptic input-output functions of neurons in the dorsal nucleus of the lateral lemniscus in Mongolian gerbils. *J Neurosci* **31**, 4511–4523.

Raman IM, Zhang S & Trussell LO (1994). Pathway-specific variants of AMPA receptors and their contribution to neuronal signaling. *J Neurosci* **14**, 4998–5010.

Ravindranathan A, Donevan SD, Sugden SG, Greig A, Rao MS & Parks TN (2000). Contrasting molecular composition and channel properties of AMPA receptors on chick auditory and brainstem motor neurons. *J Physiol* **523**, 667–684.

Reyes AD, Rubel EW & Spain WJ (1994). Membrane properties underlying the firing of neurons in the avian cochlear nucleus. *J Neurosci* **14**, 5352–5364.

Reyes AD, Rubel EW & Spain WJ (1996). *In vitro* analysis of optimal stimuli for phase-locking and time-delayed modulation of firing in avian nucleus laminaris neurons. *J Neurosci* **16**, 993–1007.

Rothman JS & Manis PB (2003). Kinetic analyses of three distinct potassium conductances in ventral cochlear nucleus neurons. *J Neurophysiol* **89**, 3083–3096.

Rubel EW & Parks TN (1988). Organization and development of the avian brain-stem auditory system. In *Brain Function*, ed. Edelman GM, Einar Gall W & Maxwell Cowan W, pp. 3–92. John Wiley & Sons, New York.

Sanchez JT, Gans D & Wenstrup JJ (2007). Contribution of NMDA and AMPA receptors to temporal patterning of auditory responses in the inferior colliculus. *J Neurosci* **27**, 1954–1963.

Sanchez JT, Wang Y, Rubel EW & Barria A (2010). Development of glutamatergic synaptic transmission in binaural auditory neurons. *J Neurophysiol* **104**, 1774–1789.

Scott LL, Mathews PJ, Golding NL (2005). Post hearing developmental refinement of temporal processing in principal neurons of the medial superior olive. *J Neurosci* **25**, 7887–7895.

Seidl AH, Rubel EW & Harris DM (2010). Mechanisms for adjusting interaural time differences to achieve binaural coincidence detection. *J Neurosci* **30**, 70–80.

Sivaramakrishnan S & Oliver DL (2006). Neuronal responses to lemniscal stimulation in laminar brain slices of the inferior colliculus. *J Assoc Res Otolaryngol* **7**, 1–14.

Slee SJ, Higgs MH, Fairhall AL & Spain WJ (2010). Tonotopic tuning in a sound localization circuit. *J Neurophysiol* **103**, 2857–2875.

Sobczyk A, Scheuss V & Svoboda K (2005). NMDA receptor subunit-dependent $[Ca^{2+}]$ signaling in individual hippocampal dendritic spines. *J Neurosci* **25**, 6037–6046.

Sorensen SA & Rubel EW (2006). The level and integrity of synaptic input regulates dendrite structure. *J Neurosci* **26**, 1539–1550.

Steinert JR, Postlethwaite M, Jordan MD, Chernova T, Robinson SW & Forsythe ID (2010). NMDAR-mediated EPSCs are maintained and accelerate in time course during maturation of mouse and rat auditory brainstem *in vitro*. *J Physiol* **588**, 447–463.

Stevens CF & Wang Y (1995). Facilitation and depression at single central synapses. *Neuron* **14**, 795–802.

Stocca G & Vicini S (1998). Increased contribution of NR2A subunit to synaptic NMDA receptors in developing rat cortical neurons. *J Physiol* **507**, 13–24.

Sung MJ, Ahn HS, Hahn SJ & Choi BH (2008). Open channel block of Kv3.1 currents by fluoxetine. *J Pharmacol Sci* **106**, 38–45.

Tang YZ & Carr CE (2004). Development of NMDA R1 expression in chicken auditory brainstem. *Hear Res* **191**, 79–89.

Tang YZ & Carr CE (2007). Development of N-methyl -D-aspartate receptor subunits in avian auditory brainstem. *J Comp Neurol* **502**, 400–413.

Tang ZQ, Dinh EH, Shi W & Lu Y (2011). Ambient GABA-activated tonic inhibition sharpens auditory coincidence detection via a depolarizing shunting mechanism. *J Neurosci* **31**, 6121–6131.

Taschenberger H, von Gersdorff H (2000). Fine-tuning an auditory synapse for speed and fidelity: developmental changes in presynaptic waveform, EPSC kinetics, and synaptic plasticity. *J Neurosci* **20**, 9162–9173.

Traynelis SF, Wollmuth LP, McBain CJ, Menniti FS, Vance KM, Ogden KK, Hansen KB, Yuan H, Myers SJ & Dingledine R (2010). Glutamate receptor ion channels: structure, regulation, and function. *Pharmacol Rev* **62**, 405–496.

Trussell L (1998). Control of time course of glutamatergic synaptic currents. *Prog Brain Res* **116**, 59–69.

Trussell LO (1999). Synaptic mechanisms for coding timing in auditory neurons. *Annu Rev Physiol* **61**, 477–496.

Wang LY, Gan L, Forsythe ID & Kaczmarek LK (1998). Contribution of the Kv3.1 potassium channel to high frequency firing in mouse auditory neurones. *J Physiol* **509**, 183–194.

Wu SH, Ma CL & Kelly JB (2004). Contribution of AMPA, NMDA, and $GABA_A$ receptors to temporal pattern of postsynaptic responses in the inferior colliculus of the rat. *J Neurosci* **24**, 4625–4634.

Yashiro K & Philpot BD (2008). Regulation of NMDA-R subunit expression and its implication for LTD, LTP and metaplasticity. *Neuropharmacol* **55**, 1081–1094.

Author contributions

J.T.S., E.W.R. and A.B. contributed to the conception and design of experiments. J.T.S. and A.H.S. collected the data. J.T.S. and A.B. analysed and interpreted the data. J.T.S., E.W.R. and A.B. wrote the manuscript. All authors approved the final version.

Acknowledgements

This work was supported by research grant R01 DC03829, National Research Service Award F32 DC010307, Research Core Center DC04661 from the National Institute on Deafness and Other Communication Disorders of the US Public Health Service and from the National Organization for Hearing Research.